Molecular Pharmacology Fast Forward. Published on August 9, 2022 as DOI: 10.1124/molpharm.122.000543
This article has not been copyedited and formatted. The final version may differ from this version.

Analgesic α-Conotoxin Binding Site on the Human $GABA_B$ Receptor

Anuja R. Bony, Jeffrey R. McArthur, Akari Komori, Ann R. Wong, Andrew Hung, and David J. Adams

Illawarra Health & Medical Research Institute (IHMRI), University of Wollongong, Wollongong, NSW 2522 Australia (A.R.B., J.R.M., D.J.A.);
School of Science, RMIT University, Melbourne, Victoria 3000 Australia (A.K., A.H.);
School of Health and Biomedical Sciences, RMIT University, Bundoora, Victoria 3083 Australia (A.R.W)

Running title: α-Conotoxin Binding Site on the $GABA_B$ Receptor

Corresponding authors: David J. Adams, Illawarra Health & Medical Research Institute (IHMRI), University of Wollongong, Northfields Avenue, Wollongong, NSW 2522, Australia.
ORCID iD: 0000-0002-7030-2288; Email: djadams@uow.edu.au
Andrew Hung, School of Science, RMIT University, Melbourne, Victoria 3000, Australia
Email: Andrew.hung@rmit.edu.au

Number of text pages: 32
Number of tables: 1
Number of figures: 8
Number of references: 47
Number of words – *Abstract*: 244
Introduction: 705
Discussion: 1493

Molecular Pharmacology Fast Forward. Published on August 9, 2022 as DOI: 10.1124/molpharm.122.000543
This article has not been copyedited and formatted. The final version may differ from this version.

Abstract

The analgesic α-conotoxins Vc1.1, RgIA, and PeIA attenuate nociceptive transmission via activation of G protein-coupled $GABA_B$ receptors ($GABA_BR$) to modulate N-type calcium channels in primary afferent neurons and recombinantly co-expressed human $GABA_BR$ and Cav2.2 channels in HEK293T cells. Here, we investigated the effects of analgesic α-conotoxins following the mutation of amino acid residues in the Venus Flytrap (VFT) domains of the $GABA_BR$ subunits predicted through computational peptide docking and molecular dynamics simulations. Our docking calculations predicted that all three of the α-conotoxins form close contacts with VFT residues in both B1 and B2 subunits, comprising a novel $GABA_BR$ ligand-binding site. The effects of baclofen and α-conotoxins on the peak Ba^{2+} current (I_{Ba}) amplitude were investigated on wild-type and 15 $GABA_BR$ mutants individually co-expressed with human Cav2.2 channels. Mutations at the interface of the VFT domains of both $GABA_BR$ subunits attenuated baclofen-sensitive I_{Ba} inhibition by the analgesic α-conotoxins. In contrast, mutations located outside the putative peptide-binding site (D380A and R98A) did not. The key $GABA_BR$ residues involved in interactions with the α-conotoxins are K168 and R207 on the B2 subunit and S130, S153, R162, E200, F227, and E253 on the B1 subunit. The double mutant, S130A+S153A, abolished inhibition by both baclofen and the α-conotoxins. Depolarization-activated I_{Ba} mediated by both wild-type and all $GABA_BR$ mutants were inhibited by the selective $GABA_BR$ antagonist CGP 55845. This study identifies specific residues of $GABA_BR$ involved in the binding of the analgesic α-conotoxins to the VFT domains of the $GABA_BR$.

Molecular Pharmacology Fast Forward. Published on August 9, 2022 as DOI: 10.1124/molpharm.122.000543
This article has not been copyedited and formatted. The final version may differ from this version.

Significance Statement

This study defines the binding site of the analgesic α-conotoxins Vc1.1, RgIA, and PeIA on the human $GABA_B$ receptor to activate Gi/o proteins and inhibit Cav2.2 channels. Computational docking and MD simulations of $GABA_BR$ identified amino acids of the Venus flytrap (VFT) domains with which the α-conotoxins interact. $GABA_BR$ alanine mutants attenuated baclofen-sensitive Cav2.2 inhibition by the α-conotoxins. We identify an allosteric binding site at the interface of the VFT domains of the $GABA_BR$ subunits for the analgesic α-conotoxins.

Abbreviations: BSA, bovine serum albumin; cryo-EM, cryogenic electron microscopy; DAPI, 4′,6-diamidino-2-phenylindole; DRG, dorsal root ganglion; eGFP, enhanced green fluorescent protein; MD, molecular dynamics; $GABA_BR$, G protein-coupled γ-aminobutyric acid type B receptor; HEK, human embryonic kidney; nAChR, nicotinic acetylcholine receptor; PBS, phosphate buffer saline; PCT, proximal carboxyl terminus; 7TM, seven-helix transmembrane domain; VFT, Venus flytrap; WT, wild-type.

Keywords: Conotoxins, $GABA_B$ receptor, voltage-gated calcium channels, computational peptide docking, molecular dynamics simulations, site-directed mutagenesis, allosteric binding site, patch clamp recording

Molecular Pharmacology Fast Forward. Published on August 9, 2022 as DOI: 10.1124/molpharm.122.000543
This article has not been copyedited and formatted. The final version may differ from this version.

Introduction

Marine cone snail venom is a rich source of peptides called conotoxins that have evolved for defense and prey capture. α-Conotoxins are disulfide-bonded peptides that antagonize nicotinic acetylcholine receptors (nAChR) in the central and peripheral nervous systems and many exhibit exquisite selectivity for nAChR subtypes (Abraham and Lewis, 2018; Azam and McIntosh, 2009; Lebbe et al., 2014). α-Conotoxins Vc1.1, RgIA, and PeIA selectively inhibit the α9α10 nAChR subtype (Daly et al., 2011; Ellison et al., 2008; McIntosh et al., 2005; Nevin et al., 2007) and were shown to be anti-nociceptive in animal pain models (Hone et al., 2018; McIntosh et al., 2009; Mohammadi and Christie, 2015; Vincler et al., 2006). These analgesic α-conotoxins were subsequently shown to indirectly inhibit high voltage-activated (HVA) N-type calcium channels by activating $GABA_B$ receptor ($GABA_BR$) coupled, pertussis toxin-sensitive Gi/o proteins in rodent dorsal root ganglion (DRG) neurons (Callaghan et al., 2008; Callaghan & Adams, 2010; Daly et al., 2011). Knockdown of $GABA_BR$ expression in rat DRG neurons reduced the activity of Vc1.1 and Rg1A and could be reconstituted in HEK 293 cells expressing human $GABA_BR$ and Cav2.2. Furthermore, inhibition of human (h) Cav2.2 channels by Vc1.1 and RgIA required the expression of both B1 and B2 receptor subunits and the selective $GABA_BR$ antagonist CGP55845 blocked the modulation by α-conotoxins (Cuny et al., 2012).

α-Conotoxin Vc1.1 modulation of Cav2.2 is via a site distinct from the orthosteric $GABA_BR$ binding site for agonists, γ-aminobutyric acid (GABA) and baclofen. The $GABA_BR$ agonists typically bind to the B1 Venus flytrap domain, which then activates the $GABA_BR$, leading to inhibition of Cav2.2 channels via a pathway involving Gβγ subunits (Galvez et al., 1999). The binding of Gβγ to Cav2.2 modifies it from a "willing" to "reluctant" gating state, thus shifting inactivation to more hyperpolarized potentials while slowing activation kinetics (Zamponi and Currie, 2013). Vc1.1 modifies Cav2.2 channel

Molecular Pharmacology Fast Forward. Published on August 9, 2022 as DOI: 10.1124/molpharm.122.000543
This article has not been copyedited and formatted. The final version may differ from this version.

kinetics through a distinct mechanism from the classical $GABA_BR$ agonists (increased activation rate and hyperpolarized shift in half-maximum inactivation) (Huynh et al., 2015). Cav2.2 channels in HEK293T cells co-expressing hCav2.2 and $GABA_BR$ constructs were inhibited by Vc1.1 with mutations that abolish GABA/baclofen binding (B1-S270A and B1-S246A) (Huynh et al., 2015). This finding suggested that Vc1.1 could act at an allosteric site on $GABA_BRs$. In DRG neurons, selective $GABA_BR$ antagonists, CGP54626 and CGP55845, blocked Vc1.1 modulation of Cav2.2-mediated currents (Callaghan et al., 2008; Callaghan & Adams, 2010). However, in HEK293 cells expressing $GABA_{B1}$-S270A that attenuates CGP54626 binding (Galvez et al., 1999; Geng et al., 2013), this compound was unable to antagonize Vc1.1 inhibition of Cav2.2 (Huynh et al., 2015). This suggests that CGP54626 and CGP55845 either act allosterically to inhibit Vc1.1 binding or bridge the orthosteric pocket and an allosteric site (distinct from S270 and S246 of B1).

Recent cryo-EM studies of the $GABA_BR$ have been elucidated for the receptor bound to a variety of different ligands. The observed structures capture alternate conformations from the inactive *apo* state to the fully active G protein-bound state (see Shaye et al., 2021). The N-terminal extracellular domains of B1 and B2, each consist of two lobes, LB1 and LB2, of the "Venus Flytrap domains" (VFTs), which trap the ligand in its orthosteric binding site situated on B1 at the B1/B2 interface. Previous structural studies of the $GABA_BR$ suggest both agonists and antagonists are anchored by a set of polar residues and a key aromatic residue (W182) of LB1. Upon agonist binding, the two lobes close while engaging two bulky aromatic LB2 residues sandwiching the ligand (Geng et al., 2012; 2013). Two major receptor conformations, active and inactive, as well as two intermediate states, have been observed in cryo-EM structures providing insights into the activation pathway of the $GABA_BR$ upon activation by agonists (Shaye et al., 2020).

Molecular Pharmacology Fast Forward. Published on August 9, 2022 as DOI: 10.1124/molpharm.122.000543
This article has not been copyedited and formatted. The final version may differ from this version.

The present study used computational docking studies and molecular dynamics simulations, with the crystal structures of the $GABA_BR$ VFT subunits as templates, to identify amino acid residues with which α-conotoxins Vc1.1, RgIA, and PeIA likely interact. These residues were mutated to investigate their impact on the activation of the $GABA_BR$ by the different ligands, as determined by inhibition of hCav2.2 channels expressed in HEK293T cells. We identify an allosteric binding site at the interface of the VFT domains of the $GABA_BR$ subunits for the analgesic α-conotoxins.

Materials and Methods

Computational peptide docking.

Conotoxin-receptor complex structures were predicted via molecular docking using Autodock Vina (Eberhardt et al., 2021; Trott and Olson, 2010). The $GABA_BR$ extracellular VFT structure was used as the receptor (PDB ID: 4MQF, resolution 2.22 Å; Supplemental Data PDB file: PDB 1 (Apo)) (Geng et al., 2013). The α-conotoxin structures used were obtained as follows: Vc1.1 (PDB ID: 2H8S) (Clark et al., 2006), RgIA (PDB ID: 2JUT) (Ellison et al., 2008), PeIA (PDB ID: 5JME) (Daly et al., 2011), and ImI (PDB ID: 1G2G) (Lamthanh et al., 1999). Discovery Studio Visualizer (BIOVIA, Dassault Systèmes, Discovery Studio Visualizer, 2021, San Diego, CA) was used to modify parent conotoxins to create the analogue RgIA4. The $GABA_BR$ and all conotoxin structures were converted to PDBQT format using PyRx (Dallakyan and Olson, 2015), the graphical frontend for Autodock Vina. $GABA_BR$ torsion angles were treated as fixed. Conotoxin backbone torsion angles were fixed, while amino acid sidechain torsion angles were set as flexible. The Vina grid box was centered on $GABA_BR$ and set with x, y, z dimensions of 82.4 Å x 77.6 Å x 84.5 Å, covering the entire accessible surface of the receptor. The exhaustiveness parameter was set to 256 for all dockings. 2D ligand-receptor interaction diagrams were produced using

Molecular Pharmacology Fast Forward. Published on August 9, 2022 as DOI: 10.1124/molpharm.122.000543
This article has not been copyedited and formatted. The final version may differ from this version.

Schroedinger Maestro (Schrödinger Release 2021-4: Maestro, Schrödinger, LLC, New York, NY). The most favourable docking poses were selected for prediction of $GABA_BR$ residues implicated in conotoxin binding, which guided subsequent experimental mutagenesis and electrophysiology studies. The stereochemical quality of all models were evaluated using PROCHECK (Laskowski et al., 1993) and VERIFY3D (Bowie et al., 1991; Lüthy et al., 1992) accessed via the SAVES v6.0 server (saves.mbi.ucla.edu), and with ProSA-Web (Sippl, 1993; Wiederstein and Sippl, 2007). Model quality statistics are presented in Table S1. Structural files in PDB format for the top docking-predicted models of Vc1.1, RgIA, PeIA, and RgIA4 bound to the $GABA_BR$ VFT are provided in Supplemental Data PDB files, PDB 2 (Vc1.1), PDB 4 (RgIA), PDB 5 (PeIA), and PDB 2 (RgIA4), respectively. The top eight energetically favoured docking-predicted models for ImI bound to the $GABA_BR$ VFT are provided in Supplemental Data PDB files, PDB 2 (ImI - model 1), PDB 3 (ImI - model 2), PDB 11 (ImI - model 3), PDB 10 (ImI - model 4), PDB 9 (ImI - model 5), PDB 8 (ImI - model 6), PDB 7 (ImI - model 7), and PDB 6 (ImI - model 8).

Molecular dynamics simulations.

Energetically-favoured binding poses for the VFT of $GABA_BR$ bound to Vc1.1, RgIA, or PeIA, predicted using docking as described above, were used for subsequent all-atom fully-solvated molecular dynamics (MD) simulations. Each conotoxin-receptor complex was placed in a dodecahedron periodic box of dimensions 124 Å x 24 Å x 124 Å. Each box was filled with 39612 TIP3P water molecules (Jorgensen et al., 1983). Approximately 128 Na^+ and 122 Cl^- ions were added to neutralise the charge and produce an approximate ionic concentration of 150 mM. Simulations were performed using GROMACS 2019 (Van Der Spoel et al., 2005; Pronk et al., 2013) and the CHARMM36m forcefield (Huang et al., 2017). The integration time step was set to 2 fs. Van der Waals interactions were switched to zero

Molecular Pharmacology Fast Forward. Published on August 9, 2022 as DOI: 10.1124/molpharm.122.000543
This article has not been copyedited and formatted. The final version may differ from this version.

between 0.8 and 1.2 nm. Electrostatic interactions were evaluated using the fast smooth particle-mesh Ewald (PME) method (Essmann et al., 1995) with a Coulombic potential cut-off of 1.2 nm. Covalent bonds involving hydrogen atoms were constrained using the LINCS algorithm (Hess et al., 1997). For the restraint-free simulations, the velocity rescale thermostat of Bussi et al. (2007), with a coupling time constant of 0.1 ps, was used to maintain the temperature of all simulations at 310 °K. The pressure was maintained at 1 bar using isotropic coupling with the Parrinello-Rahman barostat algorithm (Parrinello and Rahman, 1981). The systems were firstly energy minimized using the steepest descent algorithm for a maximum of 10,000 steps. Each system was equilibrated by running positional-restraint simulations in which all non-solvent heavy atoms were positionally restrained, firstly under a constant particle number, velocity, and temperature (NVT) ensemble for 100 ps, followed by a constant particle number, pressure, and temperature (NPT) simulation for another 100 ps. Subsequently, all restraints were removed and 1000 ns equilibrium simulations were performed for each of the three α-conotoxin-$GABA_BR$ systems, as well as the apo VFT, producing a total of 4 μs worth of trajectories. Molecular structures were visualized using Visual Molecular Dynamics version 1.9.3 (VMD) (Humphrey et al., 1996).

HEK293T cell culture and transfection.

HEK293 cells expressing large SV40 T antigens (HEK293T) were obtained from American Type Cell Culture Collection (ATCC® CRL-3216, RRID: CVCL_0063), Virginia, USA. HEK293T cells were cultured in Dulbecco's modified Eagle's medium (DMEM, Invitrogen™, Thermofisher Scientific, Mulgrave, VIC, Australia) containing 10% foetal bovine serum (GIBCO™, Thermofisher Scientific), 1% penicillin and streptomycin (Pen/Strep, Invitrogen™, Thermofisher Scientific) and 1% GlutaMAX (Invitrogen™,

Molecular Pharmacology Fast Forward. Published on August 9, 2022 as DOI: 10.1124/molpharm.122.000543
This article has not been copyedited and formatted. The final version may differ from this version.

Thermofisher Scientific). Cells were incubated in 5% CO_2 at 37°C in a humidified incubator and passaged at 10% original density to when ~80% confluency was reached.

HEK293T cells were transiently co-transfect with plasmid cDNAs encoding human Cav2.2 channels (subunits α_{1B}-e37b, α2δ1, and β3; each subunit 2 μg; OriGene Technologies, Inc., Rockville, MD, USA) and either tricistronic human $GABA_{B1}$, $GABA_{B2}$ with enhanced green fluorescent protein (eGFP, 2 μg; custom-designed clone of Adams Lab) (wild-type $GABA_BR$) or mutants of $GABA_BR$ also tagged with eGFP (2 μg; GenScript, Piscataway, New Jersey, USA) using calcium phosphate transfection (Kumar et al, 2019). Cells were plated on 12 mm glass coverslips and incubated with calcium DNA precipitation mix in growth media at 37°C for 16-18 hours. Afterward, upon changing the transfection media to fresh cell culture media, they were transferred to a 30°C incubator with 5% CO_2. 48-72 hours post-transfection cells were used at room temperature (22-24°C) to conduct experiments.

Patch clamp electrophysiology.

Whole-cell voltage clamp recordings were acquired using a MultiClamp 700B amplifier and digitized through Digidata 1440A (Molecular Devices, San Jose, CA, USA). Data were obtained using pClamp 11 (Molecular Devices) software while maintaining series resistance to <10 MΩ, and the cell capacitance compensated by ≥80%. The external bath solution to record $GABA_BR$-coupled Cav2.2-mediated currents contained (mM): 100 NaCl, 10 $BaCl_2$, 1 $MgCl_2$, 5 CsCl, 30 TEA-Cl, 10 D-Glucose and 10 HEPES, pH adjusted to 7.35 using TEA-OH and ~320 $mOsmol.kg^{-1}$. Patch pipettes were filled with internal solution containing (in mM): 120 Kgluconate, 5 NaCl, 2 $MgCl_2$, 5 EGTA, 10 HEPES, 5 MgATP and 0.2 Na_2GTP, pH adjusted to 7.2 using KOH, ~295 $mOsmol.kg^{-1}$and had resistance of 1-3 MΩ.

Whole-cell peak Ba^{2+} currents (I_{Ba}) were elicited by a test pulse to 0 mV from a holding potential (V_h) of –90 mV, sampled at 10 kHz, filtered at 1 kHz, and leak current subtracted using a –P/4 pulse protocol. Whole-cell Cav2.2-mediated I_{Ba} is normalized to the baclofen-

Molecular Pharmacology Fast Forward. Published on August 9, 2022 as DOI: 10.1124/molpharm.122.000543
This article has not been copyedited and formatted. The final version may differ from this version.

sensitive component to eliminate expression artifacts associated with transient transfection of HEK293T cells with human $GABA_B$ receptor subunits and Cav2.2 channels. All solutions including the drugs (peptides, baclofen, and CGP 55845) were perfused using a peristaltic pump at an exchange speed of 1 $ml.min^{-1}$ in an experimental chamber (~0.5 ml volume) at room temperature.

Immunocytochemistry.

HEK293T cells were transfected with Cav2.2 and $GABA_BR$ or the mutants of $GABA_BRs$ tagged with eGFP using calcium phosphate transfection. After transfection, cells were washed twice with 1x Phosphate Buffer Saline (PBS), pH 7.4 for 5 min and fixed with Zamponi's solution containing 1.6% formaldehyde (Australian Biostain Pty Ltd., Traralgon, VIC, Australia). Immunostaining was performed using the indirect fluorescence method. The primary antibodies and their dilution used for the receptor subunits were anti-$GABA_BR1$ (goat, 1: 250; Santa Cruz Biotechnology, Dallas, TX, USA; sc-7338) and anti-$GABA_BR2$ (rabbit, 1: 250; Santa Cruz Biotechnology; sc-28792). They were visualized consequently with Alexa Fluor 647-conjugated donkey anti-goat antibody (1: 500; Life technology, A21447) and Alexa Fluor 555-conjugated goat anti-rabbit (1:500; Abcam, ab150078). Before staining, cells were permeabilized with 0.1% Triton X-100 for 10 min and blocked for 1 h with a PBS-based blocking solution containing 1g Bovine Serum Albumin (BSA) and 0.1% Triton X-100. For double immunostaining of the receptor subunits, primary antibodies were added simultaneously and incubated at 4^oC overnight, rinsed in three changes of PBS (10 min each), and then incubated sequentially for Alexa Fluor 647-conjugated donkey anti-goat antibody followed by Alexa Fluor 555-conjugated goat anti-rabbit; each for 1 h at room temperature (RT). Negative controls were carried out by omitting the primary antibodies in transfected HEK293T cells and by including the primary antibodies in non-transfected HEK293T cells. All coverslips were counterstained with DAPI (1:5000, 10 min, RT),

Molecular Pharmacology Fast Forward. Published on August 9, 2022 as DOI: 10.1124/molpharm.122.000543
This article has not been copyedited and formatted. The final version may differ from this version.

mounted (Dako North America Inc., Carpinteria, CA, USA), sealed, and stored at 4°C. Images were obtained using Leica SP8 confocal microscope (Leica Microsystem Pty Ltd., Macquarie Park, NSW, Australia) using a 40x oil immersion objective and analyzed using Las X software (RRID:SCR_013673, Leica microsystem).

Data analysis and statistics.

Patch clamp electrophysiology data are reported as mean ± SEM and n is the number of individual experiments. The significance of peptides effects among different mutants of $GABA_BR$ was compared to the wild-type (WT) $GABA_BR$ group. Therefore, multiple comparisons were performed by one-way ANOVA followed by Dunnett's post hoc test. Values of $P < 0.05$ were considered significant. Clampfit 11 (Molecular Devices, San Jose, CA, USA) and GraphPad Prism 9 (San Diego, CA, USA) software were used to analyze the data.

Control currents were obtained by measuring the peak steady-state whole-cell I_{Ba} ($I_{control}$), peak inhibition of peptides, Vc1.1, Rg1A, and PeIA ($I_{peptide}$) by applying saturating concentrations, and finally, applying a saturating concentration of baclofen (50 μM; I_{Bac}) was used to isolate the baclofen-sensitive currents. To calculate baclofen-sensitive inhibition of $GABA_BR$-coupled Cav2.2 currents by each peptide, we used the following formula:

$$\text{Baclofen inhibition} = (I_{control} - I_{Bac}) / I_{control}$$

$$\text{Inhibition by peptides} = (I_{control} - I_{peptide}) / I_{control}$$

$$\%\ \text{Inhibition of baclofen-sensitive current by peptide} = (I_{peptide}/I_{Bac}) \times 100$$

Notably, the selective $GABA_BR$ antagonist, CGP 55845, was applied at the end of each experiment to validate $GABA_BR$ inhibition by peptides and/or baclofen.

Results

Molecular docking, simulations, and identification of α-conotoxin-VFT interactions.

Molecular Pharmacology Fast Forward. Published on August 9, 2022 as DOI: 10.1124/molpharm.122.000543
This article has not been copyedited and formatted. The final version may differ from this version.

The initial binding positions of α-conotoxins Vc1.1, RgIA, and PeIA interacting with the VFT of the $GABA_BR$ were predicted using automated molecular docking calculations. The docking calculations predicted that all three of the conotoxins bind at the interface between subunits B1 and B2, as well as in the vicinity of the hinge point between lobe 1 (LB1) and lobe 2 (LB2) of both subunits. This constitutes a novel inter-subunit site for $GABA_BR$ ligand binding (Fig. 1A). While the predicted α-conotoxin binding residues include those which interact with classic agonists such as baclofen, residues predicted to interact exclusively with α-conotoxins are situated near the inter-subunit cleft in both B1 and B2 subunits (Fig. 1B).

The most energetically-favoured binding poses are shown in Fig. 2A for Vc1.1, Fig. 3A for RgIA, and Fig. 3C for PeIA. All three conotoxins form similar patterns of binding interactions with their surrounding $GABA_BR$ residues. As an illustration, the 2D ligand interaction diagram of Vc1.1 (Fig. 2C) shows all of the $GABA_BR$ residues predicted to reside within 5Å of any atom of each of the three α-conotoxins. These receptor residues comprise those which interact closely with known agonists such as baclofen and GABA and include the subunit B1 (LB1) residues S130, S131, and S154 (Geng et al., 2013). Similar interactions are identifiable from 2D ligand diagrams for RgIA (Fig. S4A) and PeIA (Fig. S4B). Additionally, a small number of residues in the B2 subunit are also involved in α-conotoxin binding. In particular, K168, in LB1, is consistently predicted to form hydrogen bonding (Vc1.1 and PeIA) or salt bridge interactions (RgIA) with all of the conotoxins.

All-atom, fully-solvated molecular dynamics (MD) simulations were subsequently performed on the three α-conotoxin-$GABA_BR$ VFT complexes to further investigate the roles of key residues of subunits B1 and B2 in facilitating receptor interactions with these toxins. The simulation trajectories for Vc1.1, RgIA, and PeIA bound to the VFT indicate that the conotoxins form strong, persistent, and stable interactions with the key B1 subunit binding site residues. The most significant contacts with B1 are shown as blue time series curves in

Molecular Pharmacology Fast Forward. Published on August 9, 2022 as DOI: 10.1124/molpharm.122.000543
This article has not been copyedited and formatted. The final version may differ from this version.

Figs. 2B, 3B, and 3D, which show relatively high numbers of inter-atomic contacts between each conotoxin and the subunit exhibiting the most persistent interaction during their respective simulation trajectories, namely, the LB1 residues S130 and S131 for Vc1.1 and PeIA, and the LB2 residue E200 for RgIA. Each of the conotoxins also forms regular, but more intermittent, contacts with the key B2 subunit residue, K168, as shown by the red time series curves in these figures.

Site-directed mutagenesis, electrophysiology, and immunocytochemistry.

Based on the initial docking calculations, residues that are predicted to form direct hydrogen bonding or salt bridge interactions with the conotoxins were selected for experimental characterization via Alanine (Ala) mutagenesis and electrophysiology studies. In addition, a subset of other residues within the vicinity of these tight-binding residues were also selected for experimental validation of their roles in conotoxin activity at $GABA_BR$. The positions of the residues selected for experimental Ala mutagenesis studies are summarised in Fig. 1 and are colour-coded according to the effects of their mutation to alanine. The effects of baclofen and α-conotoxins Vc1.1, Rg1A, and PeIA on whole-cell I_{Ba} mediated by wild-type (WT) $GABA_BR$-coupled Cav2.2 channels expressed in HEK293T cells are shown in Figs. 4 and S5. Bath application of Vc1.1, RgIA, and PeIA (1 μM) inhibited the baclofen-sensitive I_{Ba} amplitude of human Cav2.2 channels co-transfected with WT and mutant $GABA_BR$ subunits (Fig. 5). In contrast, in HEK293T cells over-expressing single Ala mutants of $GABA_BR$ B1 and B2 subunits, baclofen (50 μM) inhibition of I_{Ba} amplitude was unchanged whereas inhibition of I_{Ba} by the α-conotoxins was significantly attenuated for all mutants, except for E253A in the presence of PeIA (Fig. 5). Furthermore, two residues that were predicted to be remote from the α-conotoxin binding site, R89 and D380, were also mutated to Ala. Patch clamp recording of HEK293T cells expressing these mutants confirmed that these two residues are inconsequential for α-conotoxin activity. Overexpression of the double mutant

Molecular Pharmacology Fast Forward. Published on August 9, 2022 as DOI: 10.1124/molpharm.122.000543
This article has not been copyedited and formatted. The final version may differ from this version.

(S130A + S153A) abolished the inhibition of $GABA_BR$-coupled Cav2.2 channels by both baclofen and the α-conotoxins. In the presence of the selective $GABA_BR$ antagonist CGP55845 (1 μM), the effects of baclofen and α-conotoxins on WT and all $GABA_BR$ mutants except the double mutant (S130A + S153A) were completely abolished. A summary of the inhibition of baclofen-sensitive I_{Ba} (% $I_{peptide}/I_{baclofen}$) mediated by WT and mutant $GABA_BR$-coupled Cav2.2 channels by α-conotoxins Vc1.1, Rg1A, and PeIA is presented in Table 1.

To confirm that the $GABA_BR$ Ala mutants were expressed in the HEK293T cell membrane, commercially available antibodies were used to explore the expression and co-localization of the $GABA_BR$ subunits. Positive immunodetection and colocalization were observed for both subunits for WT and $GABA_BR$ mutants (Fig. 6; Fig. S2), including those that were predicted to form close contact with the analgesic α-conotoxins (S130A, S153A, E253A, and K168A; Fig. 6). We did not observe immunoreactivity when the primary antibodies directed to $GABA_B$ R1 and $GABA_BR2$ were omitted, or where the antibodies were used in non-transfected HEK293T cells (Fig. S3).

Negative control peptides ImI and RgIA4.

Docking calculations were also performed on the negative control peptides, α-conotoxin ImI, and the RgIA analogue, RgIA4 (Romero et al., 2017), both of which are inactive at $GABA_BR$ (Callaghan et al., 2008; Romero et al., 2017; Bony et al., 2022). Both peptides are predicted to form far fewer contacts with subunit B1, and exhibit stronger preferences for binding to B2, compared to the active conotoxins Vc1.1, RgIA, and PeIA. Fig. S1 shows all of the binding positions predicted for ImI, none of which lie within the inter-subunit region predicted (and experimentally confirmed) to be important for conotoxin activity. For RgIA4 (Fig. 7A, bottom), binding is predicted to occur near the inter-subunit region, similar to Vc1.1, RgIA (Fig. 7A, top), and PeIA. However, RgIA4 forms few contacts with the subunit

Molecular Pharmacology Fast Forward. Published on August 9, 2022 as DOI: 10.1124/molpharm.122.000543
This article has not been copyedited and formatted. The final version may differ from this version.

B1 agonist site residues S130 and S131, and instead, is skewed towards close contacts with B2. In a series of experiments testing the activity of 1 μM RgIA4 on $GABA_BR$-coupled Cav2.2 channels expressed in HEK293T cells, the baclofen-sensitive I_{Ba} amplitude was reduced to < 15% compared to Rg1A (Fig. 6B). The preferential interaction with the B2 subunit, as opposed to B1, may explain the lack of activity of RgIA4.

Molecular dynamics predictions of α-conotoxin-dependent VFT structural transitions.

To examine the impact of α-conotoxin binding on the VFT structure, the inter-lobe separation of the B1 subunit was measured using the minimum distance between I286 and E343 as a proxy, while the separation between B1-R239 and B2-E230 was calculated to represent the inter-subunit distance at the juxtamembrane region. Inter-lobe separation plots for the B1 subunits bound to Vc1.1, RgIA, and PeIA are shown in Fig. 8A. The VFT of all of the α-conotoxin-bound complexes remain open, and none are as closed as the baclofen-bound state (dashed black line). The Vc1.1-bound VFT is marginally more open than apo- and antagonist-bound VFT (blue line), while the PeIA-VFT complex is the next most open structure. In contrast, RgIA induces substantially higher separation between the lobes, resulting in a highly open B1 conformation (green line). α-Conotoxins do not substantially influence the B2 lobe, which remains similar to the initial conformation throughout (Fig. S6). Inter-subunit separation plots for the VFT dimer are shown in Fig. 8B. Vc1.1 has marginally higher inter-subunit separation than apo-VFT. Interestingly, it occasionally induces a 'closed' inter-lobe separation that is even lower than that observed experimentally for baclofen-bound VFT (blue line), particularly towards the end of the microsecond-long simulation. RgIA induces a consistently greater separation than Vc1.1. PeIA causes the most marked increase in inter-subunit separation (purple line), with complete detachment of lobe 2 between the B1 and B2 subunits beyond 400 ns.

Molecular Pharmacology Fast Forward. Published on August 9, 2022 as DOI: 10.1124/molpharm.122.000543
This article has not been copyedited and formatted. The final version may differ from this version.

Discussion

Discovery of novel allosteric sites for α-conotoxin ligand binding.

The initial binding positions of α-conotoxins Vc1.1, RgIA, and PeIA with the VFT of the $GABA_BR$ were predicted using molecular docking calculations. In contrast to the known small molecule agonists of $GABA_BR$, which bind exclusively to the B1 subunit, all three of the analgesic α-conotoxins examined form close contact with residues in both B1 and B2 subunits. (Fig. 1). These receptor residues comprise those which interact closely with known agonists such as baclofen and GABA and include the subunit B1 (LB1) residues S130, S131, and S154 (Geng et al., 2013). K168, in B2 (LB1), is consistently predicted to form hydrogen bonding (Vc1.1 and PeIA) or salt bridge interactions (RgIA).

The residues selected for experimental Ala mutagenesis studies are summarised in Fig. 1A. S130, S131, and E253 are known residues important for the activity of classical agonists, such as baclofen. Residues situated near the inter-subunit interface region in both B1 (such as F227) and B2 (K168) subunits, uniformly show significant interactions with all three α-conotoxins. Baclofen inhibition mediated by mutant $GABA_BR$-coupled Cav2.2 channels was unchanged between WT and all $GABA_B$ mutants except for the double mutant S130A+S153A. This suggests that analgesic α-conotoxins target largely different residues, and unlike baclofen, this interaction might also engage a non $G_{\beta\gamma}$-mediated voltage-independent pathway (Berecki et al., 2014).

Docking predictions for the negative controls, ImI and RgIA4, lend further support to our present proposed model, as these peptides lack the identified interactions with these residues. Residues located in LB1, such as W65, S130, G151, S153, H170, and E349, are responsible for anchoring ligands in the binding pocket and interact with both agonists and antagonists. Ligand interaction with the LB2 residue Y250 is unique for agonists, and W278 located in the same domain has been found to only interact with high-affinity antagonists in

Molecular Pharmacology Fast Forward. Published on August 9, 2022 as DOI: 10.1124/molpharm.122.000543
This article has not been copyedited and formatted. The final version may differ from this version.

addition to agonists. The binding footprint of α-conotoxins overlap those of classical ligands (Fig. 1B), including S131 and Y250 within lobes 1 and 2 of subunit B1 (coloured red in Fig. 1B), but also involves residues proximal to the B1/B2 interface (yellow in Fig. 1B).

MD simulations were performed on the three α-conotoxin-$GABA_BR$ VFT complexes to further highlight the roles of key residues of subunits B1 and B2 in facilitating receptor interactions with these toxins. The most stable contacts are formed with subunit B1 residues within the agonist pocket (such as S130 and S131), while the B2 subunit residue K168 is also closely involved in binding with α-conotoxins, albeit playing an auxiliary role in anchoring conotoxins to the novel inter-subunit/inter-lobe site. Radioligand binding studies using [^{3}H]GABA and site-directed mutagenesis show that the orthosteric binding site of $GABA_BR$ is located in the VFT of GABAB1. The binding of ligands to the VFT B2 subunit has not previously been observed, though the seven-helix transmembrane domain (7TM) of GABAB2 hosts an allosteric binding site and is responsible for G-protein coupling (Kniazeff et al., 2016). Our results suggest that the VFT B2 subunit is involved in the activation of $GABA_BR$ by α-conotoxins.

Putative VFT structural transitions and possible influences on activation pathways induced by α-conotoxin binding.

The conformation of the VFT in the extracellular domain is closely associated with the functional state of $GABA_BR$, and crystal structures indicate that both intra- and inter-subunit conformations are sensitive to ligand binding. Agonists stabilize the B1 subunit of the VFT in a 'closed' configuration, in which the two lobes of subunit B1 (LB1 and 2) encase the ligand, as in the case of baclofen (PDB ID:4MS4; Geng et al., 2013). In contrast, the apo- or antagonist-bound B1 subunit of the VFT exhibits an 'open' conformation, in which the lobes are separated (e.g. PDB ID:4MQF; Geng et al., 2013). Furthermore, the agonist-bound $GABA_BR$ exhibits close contacts between B1 and B2 in the juxtamembrane region of the

Molecular Pharmacology Fast Forward. Published on August 9, 2022 as DOI: 10.1124/molpharm.122.000543
This article has not been copyedited and formatted. The final version may differ from this version.

VFT, while *apo*- or antagonist-bound receptors induce a higher separation between the subunits.

The inter-lobe separation of the B1 subunit was measured using the minimum distance between I286 and E343 as a proxy, while the separation between B1-R239 and B2-E230 was calculated to represent the inter-subunit distance at the juxtamembrane region. Simulations revealed the promotion of VFT conformations not yet observed in experiments, which are distinct from those presently known to be stabilized by small-molecule agonists and antagonists. Binding of α-conotoxins induced higher separation between LB1 and LB2 in the B1 subunit, resulting in an 'open' conformation that exceeds that of the known apo- and antagonist-bound VFT structures (Fig. 7A). Similar structures have previously spontaneously emerged in unbiased MD simulations of the isolated B1 VFT subunit, characterized by Evenseth et al. (2020) as the 'wide open' state. In the present simulations, this 'wide open' conformation is exemplified by the RgIA-VFT complex (green line) where inter-lobe opening occurred within 100 ns of the present simulations while the apo-VFT B1 lobe retains its initial classical 'open' conformation (Fig. S6). Although Evenseth et al. (2020) cautioned against over-interpretation of the 'wide-open' conformation due to the lack of the B2 subunit in their simulations, our present work shows that association with the adjacent B2 subunit does not hinder the emergence of this predicted B1 conformation. There is little influence of α-conotoxin binding on the inter-lobe separation of B2 (Fig. S7). We propose that the 'wide open' B1 conformation, being distinct from that induced by baclofen and other agonists, could trigger the alternative G protein activation pathway demonstrated by Huynh et al. (2015).

In addition to intra-subunit B1 changes, the binding of α-conotoxins may also induce increased distance between the B1 and B2 subunits in the juxtamembrane region, as exemplified by the PeIA-VFT complex (Fig. 7B, purple line), in which LB2 of both subunits

Molecular Pharmacology Fast Forward. Published on August 9, 2022 as DOI: 10.1124/molpharm.122.000543
This article has not been copyedited and formatted. The final version may differ from this version.

are fully separated during the simulation. Such a dimeric conformation has not yet been observed experimentally for $GABA_BR$. While the focus of the current work is on identifying the binding site of α-conotoxins on the VFT, we also acknowledge that the absence of the 7TM domain could influence the variability of the inter-subunit distance. However, full-length *apo* metabotropic glutamate receptor 5 (mGlu5) (Koehl et al., 2019) also exhibits a wide separation of >35 Å at the juxtamembrane region, similar to that observed for the 'open', PeIA-bound VFT conformations. Given that mGlu5 is also a class C GPCR, with a similar structural architecture, it is possible that a broad range of configurational 'openness' is also energetically accessible to $GABA_BR$ even in the presence of the 7TM and lipid membrane. Such large inter-subunit separation does not occur in our simulation of the apo-VFT (Fig. S6). Further work is required to elucidate the full impact of α-conotoxin binding on the complete structure of $GABA_BR$, including experimental determination of a complete α-conotoxin-$GABA_BR$ complex.

Most intriguing of all is the structural impact of Vc1.1 on the VFT. In the Vc1.1-VFT simulation, the binding of the toxin resulted in greater closure between the subunits B1 and B2 at the juxtamembrane region, resulting in a conformation that closely resembles the dimeric structure of the classical agonist-bound state (Fig. 7B, blue line). However, the inter-lobe separation retains an openness which closely resembles that of the classical antagonist-bound state, though less than the 'wide open' conformation present in RgIA- and PeIA-bound VFT. The Vc1.1-bound VFT structure appears to be a novel hybrid conformation composed of an 'antagonist-like' B1 subunit, but an 'agonist-like' dimer complex. The existence of this postulated hybrid state and its functional implications remain to be confirmed experimentally. Nevertheless, it suggests one structural mechanism by which binding of Vc1.1 may activate alternative G protein pathways distinct from baclofen and other agonists.

Conclusions

Molecular Pharmacology Fast Forward. Published on August 9, 2022 as DOI: 10.1124/molpharm.122.000543
This article has not been copyedited and formatted. The final version may differ from this version.

This study elucidated the main site of α-conotoxin interaction with the $GABA_BR$, showing that the three α-conotoxins studied bind to both B1 and B2 subunits in the VFT, unlike classical small-molecule agonists and antagonists whose interaction footprints are confined to B1. We propose that α-conotoxin binding at the inter-subunit cleft of the VFT may accelerate structural transformations across the dimer, including separation of the subunits at the juxtamembrane region and increase in inter-lobe distance, triggering a more loose conformation in the dimeric complex, similar to that observed for mGlu5 (Koehl et al., 2019). Such broad structural transitions appear to suggest the initial propagation of conformational shifts from the extracellular VFT to the intracellular 7TM. The downstream influences of α-conotoxin binding on the TM bundle and in particular the conformation shifts associated with coupling between Vc1.1 binding at the VFT in the extracellular space and the PCT, more than 40 Å away within the intracellular space, requires further work to elucidate. Although the present mutagenesis studies pinpoint several residues which play crucial roles in receptor activation by α-conotoxins, it cannot be discounted that these mutations may also provoke structural changes in the $GABA_BR$ which stabilize the protein in functionally unresponsive conformations, rather than directly disrupt toxin binding *per se*. Further functional studies which enable direct measurement of toxin-receptor contact, such as radiolabelled conotoxin binding assays, are required to provide definitive evidence for the binding location of α-conotoxins.

Acknowledgments

We thank Prof Patrick Sexton, Monash Institute of Pharmaceutical Sciences, Monash University, Melbourne, Australia for his insightful comments on a draft of the manuscript.

Authorship Contributions

Molecular Pharmacology Fast Forward. Published on August 9, 2022 as DOI: 10.1124/molpharm.122.000543
This article has not been copyedited and formatted. The final version may differ from this version.

Participated in research design: McArthur, Hung, and Adams

Conducted experiments: Bony, Komori, Wong, and Hung

Contributed new reagents or analytic tools: Hung, and Adams

Performed data analysis: Bony, McArthur, Wong, and Hung

Wrote or contributed to the writing of the manuscript: Bony, McArthur, Komori, Hung, and Adams

Molecular Pharmacology Fast Forward. Published on August 9, 2022 as DOI: 10.1124/molpharm.122.000543
This article has not been copyedited and formatted. The final version may differ from this version.

References

Abraham N, and Lewis RJ (2018) Neuronal nicotinic acetylcholine receptor modulators from cone snails. *Mar Drugs* **16**(6)**:** 208.

Azam L, and McIntosh JM. (2009) Alpha-conotoxins as pharmacological probes of nicotinic acetylcholine receptors. *Acta Pharmacol Sin* **30**(6)**:** 771-783.

Berecki G, McArthur JR, Cuny H, Clark RJ, and Adams DJ (2014) Differential $Ca_v2.1$ and $Ca_v2.3$ channel inhibition by baclofen and α-conotoxin Vc1.1 via $GABA_B$ receptor activation. *J Gen Physiol* **143:** 465-479.

Bony AR, McArthur JR, Finol-Urdaneta RK, and Adams DJ (2022) Analgesic α-conotoxins modulate native and recombinant GIRK1/2 channels via activation of $GABA_B$ receptors and reduce neuroexcitability. *Br J Pharmacol* **179**(1)**:** 179-198.

Bowie JU, Lüthy R, and Eisenberg D (1991) A method to identify protein sequences that fold into a known three-dimensional structure. *Science* **253**(5016): 164-170.

Bussi G, Donadio D, and Parrinello M (2007) Canonical sampling through velocity rescaling. *J Chem Physics* **126:** 014101.

Callaghan B, and Adams DJ (2010) Analgesic α-conotoxins Vc1.1 and Rg1A inhibit N-type calcium channels in sensory neurons of α9 nicotinic receptor knockout mice. *Channels* **4**(1)**:** 51-54.

Callaghan B, Haythornthwaite A, Berecki G, Clark RJ, Craik, DJ, and Adams DJ (2008) Analgesic α-conotoxins Vc1.1 and Rg1A inhibit N-type calcium channels in rat sensory neurons via $GABA_B$ receptor activation. *J Neurosci* **28**(43)**:** 10943-10951.

Clark RJ, Fischer H, Nevin ST, Adams DJ, and Craik DJ (2006) The synthesis, structural characterization, and receptor specificity of the α-conotoxin Vc1.1. *J Biol Chem* **281:** 23254-23263.

Cuny H, de Faoite A, Huynh T, Yasuda T, Berecki G, and Adams DJ (2012) γ-Aminobutyric acid type B ($GABA_B$) receptor expression needed for inhibition of N-type ($Ca_v2.2$) calcium channels by analgesic α-conotoxins. *J Biol Chem* **287:** 23948-23957.

Dallakyan S, and Olson AJ (2015) Small-molecule library screening by docking with PyRx. *Methods Mol Biol* **1263:** 243-250.

Daly NL, Callaghan B, Clark RJ, Nevin ST, Adams DJ, and Craik DJ (2011) Structure and activity of α-conotoxin PeIA at nicotinic acetylcholine receptor subtypes and $GABA_B$ receptor-coupled N-type calcium channels. *J Biol Chem.* **286**(12)**:** 10233-10237.

Eberhardt J, Santos-Martins D, Tillack AF, and Forli S (2021) AutoDock Vina 1.2.0: New Docking Methods, Expanded Force Field, and Python Bindings. *J Chem Inf Model* **61**(8)**:** 3891-3898.

Ellison M, Feng Z-P, Park AJ, Zhang X, Olivera BM, McIntosh JM, and Norton RS (2008) α-RgIA, a novel conotoxin that blocks the α9α10 nAChR: Structure and identification of key receptor-binding residues. *J Mol Biol* **377**(4)**:** 1216-1227.

Essmann U, Perera L, Berkowitz ML, Darden T, Lee H, and Pedersen LG (1995) A smooth particle mesh Ewald method. *J Chem Physics* **103:** 8577-8593.

Evenseth LSM, Ocello R, Gabrielsen M, Masetti M, Recanatini M, Sylte I, and Cavalli A (2020) Exploring conformational dynamics of the extracellular Venus flytrap domain of the $GABA_B$ receptor: A path-metadynamics study. *J Chem Inf Model* **60**(4)**:** 2294-2303.

Galvez T, Parmentier ML, Joly C, Malitschek B, Kaupmann K, Kuhn R, Bittiger H, Froestl W, Bettler B, and Pin J-P (1999) Mutagenesis and modeling of the $GABA_B$ receptor extracellular domain support a venus flytrap mechanism for ligand binding. *J Biol Chem* **274**(19)**:** 13362-13369.

Geng Y, Bush M, Mosyak L, Wang F, and Fan QR (2013) Structural mechanism of ligand activation in human $GABA_B$ receptor. *Nature* **504**(7479)**:** 254-259.

Geng Y, Xiong D, Mosyak L, Malito DL, Kniazeff J, Chen Y, Burmakina S, Quick M, Bush M, Javitch JA, Pin JP, and Fan QR (2012) Structure and functional interaction of the extracellular domain of human $GABA_B$ receptor GBR2. *Nat Neurosci* **15**(7)**:** 970-978.

Hess B, Bekker H, Berendsen HJC, and Fraaije JGEM (1997) LINCS: A linear constraint solver for molecular simulations, *J Comput Chem* **18:** 1463-1472.

Hone AJ, Servent D, and McIntosh JM (2018) α9-Containing nicotinic acetylcholine receptors and the modulation of pain. *Br J Pharmacol* **175**(11)**:** 1915-1927.

Huang J, Rauscher S, Nawrocki G, Ran T, Feig M, de Groot BL, Grubmüller H, and MacKerell AD (2017) CHARMM36m: An improved force field for folded and intrinsically disordered proteins, *Nature Methods* **14:** 71-73.

Humphrey W, Dalke A, and Schulten K (1996) VMD: visual molecular dynamics. *J Mol Graph* **14:** 33-38.

Huynh TG, Cuny H, Slesinger PA, and Adams DJ (2015) Novel mechanism of $Ca_v2.2$ inhibition revealed through α-conotoxin Vc1.1 activation of the $GABA_B$ receptor. *Mol Pharmacol.* **87:** 240-250.

Jorgensen WL, Chandrasekhar J, Madura JD, Impey RW, and Klein ML (1983) Comparison of simple potential functions for simulating liquid water. *J Chem Physics* **79:** 926-935.

Koehl A, Hu H, Feng D, Sun B, Zhang Y, Robertson MJ, Chu M, Kobilka TS, Laermans T, Steyaert J, Tarrasch J, Dutta S, Fonseca R, Weis WI, Mathiesen JM, Skiniotis G, and Kobilka BK (2019) Structural insights into the activation of metabotropic glutamate receptors. *Nature* **566:** 79-84.

Kniazeff J, Rovira X, Rondard P, and Pin J-P (2016) Activation mechanism and allosteric properties of the $GABA_B$ receptor, in *$GABA_B$ Receptor* (Colombo G ed) Chapt 6, pp 93-108, Humana Press/Springer International Publishing, Switzerland

Kumar P, Nagarajan A, and Uchil PD. (2019) Calcium Phosphate-Mediated Transfection of Eukaryotic Cells with Plasmid DNAs. *Cold Spring Harb Protoc* 2019(10). doi: 10.1101/pdb.prot095430.

Lamthanh H, Jegou-Matheron C, Servent D, Ménez A, and Lancelin JM (1999) Minimal conformation of the α-conotoxin ImI for the α7 neuronal nicotinic acetylcholine receptor recognition: correlated CD, NMR and binding studies. *FEBS Lett* **454**(3)**:** 293-298.

Laskowski RA, MacArthur MW, Moss DS, and Thornton JM (1993) PROCHECK - a program to check the stereochemical quality of protein structures. *J App Cryst.* **26:** 283-291.

Lebbe EK, Peigneur S, Wijesekara I, and Tytgat J (2014) Conotoxins targeting nicotinic acetylcholine receptors: an overview. *Mar Drugs* **12**(5)**:** 2970-3004.

Lüthy R, Bowie JU, and Eisenberg D. (1992) Assessment of protein models with three-dimensional profiles. *Nature* **356**(6364): 83-85.

McIntosh JM, Absalom N, Chebib M, Elgoyhen AB, and Vincler M (2009) Alpha9 nicotinic acetylcholine receptors and the treatment of pain. *Biochem Pharmacol* **78**(7)**:** 693-702.

McIntosh JM, Plazas PV, Watkins M, Gomez-Casati ME, Olivera BM, and Elgoyhen AB (2005) A novel α-conotoxin, PeIA, cloned from *Conus pergrandis*, discriminates between rat α9α10 and α7 nicotinic cholinergic receptors. *J Biol Chem* **280**(34)**:** 30107-30112.

Mohammadi SA, and Christie MJ (2015) Conotoxin interactions with α9α10-nAChRs: Is the α9α10-nicotinic acetylcholine receptor an important therapeutic target for pain management? *Toxins (Basel)* **7**(10)**:** 3916-3932.

Nevin ST, Clark RJ, Klimis H, Christie MJ, Craik DJ, and Adams DJ. (2007) Are a9a10 nicotinic acetylcholine receptors a pain target for a-conotoxins? *Mol Pharmacol* **72**(6)**:** 1406-1410.

Parrinello M, and Rahman A (1981) Polymorphic transitions in single crystals: A new molecular dynamics method. *J Appl Phys* **52:** 7182.

Pronk S, Páll S, Schulz R, Larsson P, Bjelkmar P, Apostolov R, Shirts MR, Smith JC, Kasson PM, van der Spoel D, Hess B, and Lindahl E (2013) GROMACS 4.5: A high-throughput and highly parallel open source molecular simulation toolkit. *Bioinformatics* **29:** 845-854.

Romero HK, Christensen SB, Di Cesare Mannelli L, Gajewiak J, Ramachandra R, Elmslie KS, Vetter DE, Ghelardini C, Iadonato SP, Mercado JL, Olivera BM, and McIntosh JM (2017) Inhibition of α9α10 nicotinic acetylcholine receptors prevents chemotherapy-induced neuropathic pain. *Proc Natl Acad Sci U S A.* **114**(10)**:** E1825-E1832.

Shaye H, Ishchenko A, Lam JH, Han GW, Xue L, Rondard P, Pin JP, Katritch V, Gati C, and Cherezov V (2020) Structural basis of the activation of a metabotropic GABA receptor. *Nature*. **584**(7820)**:** 298-303.

Shaye H, Stauch B, Gati C, and Cherezov V (2021). Molecular mechanisms of metabotropic $GABA_B$ receptor function. *Sci Adv*. **7**(22)**:** eabg3362.

Sippl MJ (1993) Recognition of errors in three-dimensional structures of proteins. *Proteins* **17:** 355-362.

Trott O, and Olson AJ (2010) AutoDock Vina: improving the speed and accuracy of docking with a new scoring function, efficient optimization, and multithreading. *J Comput Chem* **31**(2)**:** 455-461.

Van Der Spoel D, Lindahl E, Hess B, Groenhof G, Mark AE, and Berendsen HJC (2005) GROMACS: Fast, flexible, and free. *J. Comput. Chem*. **26:** 1701-1718.

Vincler M, Wittenauer S, Parker R, Ellison M, Olivera BM, and McIntosh JM (2006) Molecular mechanism for analgesia involving specific antagonism of α9α10 nicotinic acetylcholine receptors. *Proc Natl Acad Sci U S A.* **103**(47)**:** 17880-17884.

Wiederstein M, and Sippl MJ (2007) ProSA-web: interactive web service for the recognition of errors in three-dimensional structures of proteins. *Nucleic Acids Res* **35**, W407-W410.

Zamponi GW, and Currie KPM (2013) Regulation of Ca_V2 calcium channels by G protein coupled receptors. *Biochim Biophys Acta - Biomembranes* **1828**(7)**:** 1629-1643.

Molecular Pharmacology Fast Forward. Published on August 9, 2022 as DOI: 10.1124/molpharm.122.000543
This article has not been copyedited and formatted. The final version may differ from this version.

Footnotes

This work was supported by an Australian National Health and Medical Research Council (NHMRC) Program Grant (APP1072113) to D.J.A. J.R.M is supported by a Rebecca Cooper Foundation for Medical Research Grant (PG2019396). We thank the National Computational Infrastructure (NCI), which is supported by the Australian Government, and the Pawsey Supercomputing Centre, supported by the Western Australian Government and the Australian Government, and the University of Melbourne Research Computing Services facilities, for providing resources and services to enable the computational work in this study. A.R.W. acknowledges financial support through the Australian Government Research Training Program (RTP) Scholarship.

No author has an actual or perceived conflict of interest with the contents of this article.

Molecular Pharmacology Fast Forward. Published on August 9, 2022 as DOI: 10.1124/molpharm.122.000543
This article has not been copyedited and formatted. The final version may differ from this version.

Figure Legends

Fig. 1. $GABA_BR$-Vc1.1 structure, illustrating residues targeted for mutagenesis studies and comparison with the baclofen binding site. Computational docking predicted binding of Vc1.1 (blue ribbon) at the inter-subunit region of the VFT in ribbon representation (B1 = transparent blue, B2 = transparent red). Residues predicted to form close contacts with α-conotoxin Vc1.1, RgIA, and PeIA and whose Ala mutants result in significantly reduced inhibition of baclofen-sensitive Cav2.2-mediated current are shown as orange spheres, whereas mutant residues resulting in significantly reduced inhibition are shown as yellow spheres. Negative control residues whose mutants exert negligible effect on baclofen-sensitive Cav2.2-mediated currents are shown as grey spheres. **(B)** Baclofen (large spheres), agonist-binding residues (pink sticks) and residues that interact exclusively with α-conotoxins but not with classical agonists and antagonists (grey sticks).

Fig. 2. Predicted binding site and close-contact $GABA_BR$ residues for Vc1.1. **(A)** α-Conotoxin Vc1.1 (blue ribbon) bound at the inter-subunit region between B1 (light blue ribbons) and. B2 (light red ribbons). $GABA_BR$ residues predicted to form direct, close contact with Vc1.1 are shown as large spheres and coloured according to conventional molecular modelling schemes (red = oxygen, cyan = carbon, blue = nitrogen, white = hydrogen). **(B)** All-atom MD simulation-acquired time series plots of the B1 (blue line) and B2 (red line) residues which maintain the highest number of persistent contacts with Vc1.1, with number of toxin-receptor residue contacts plotted along the abscissa and simulation time along the ordinate. **(C)** 2-Dimensional ligand-receptor interaction diagram indicating Vc1.1 (standard molecular representation) and $GABA_BR$ residues within 5Å. Receptor residues are labelled with 3-letter codes and position numbers, and colour coded according to physicochemical properties (red = acidic, purple = basic, blue = polar, green = non-polar). Coloured lines indicate hydrogen bonding or salt-bridge interactions. Residues selected for experimental mutagenesis studies are those forming hydrogen bonds with Vc1.1 and/or within close vicinity of such residues, and are boxed with blue (B1) or red (B2) outlines.

Molecular Pharmacology Fast Forward. Published on August 9, 2022 as DOI: 10.1124/molpharm.122.000543
This article has not been copyedited and formatted. The final version may differ from this version.

Fig 3. Predicted binding site and close-contact $GABA_BR$ residues for RgIA and PeIA.
(A) α-Conotoxin RgIA (green ribbon) bound at the inter-subunit region between B1 (light blue ribbons) and. B2 (light red ribbons). $GABA_BR$ residues predicted to form direct, close contact with RgIA are shown as large spheres and coloured according to conventional molecular modelling schemes (red = oxygen, cyan = carbon, blue = nitrogen, white = hydrogen). **(B)** All-atom MD simulation-acquired time series plots of the B1 (blue line) and B2 (red line) residues which maintain the highest number of persistent contacts with RgIA, with number of toxin-receptor residue contacts plotted along the abscissa and simulation time along the ordinate. **(C)** α-Conotoxin PeIA (purple ribbon) bound at the inter-subunit region between B1 and B2. **(D)** Time series plots of the B1 (blue line) and B2 (red line) residues which maintain the highest number of persistent contacts with PeIA.

Fig. 4. Inhibition of whole-cell Ba^{2+} current mediated by wild-type $GABA_BR$-coupled Cav2.2 channels by baclofen and α-conotoxins Vc1.1, Rg1A, and PeIA. Paired scatter plots showing the correlation of percent I_{Ba} inhibition by 50 μM baclofen (red) and 1 μM Vc1.1 (**A,** blue), Rg1A (**B**, green), and PeIA (**C**, purple). Data represent mean ± SEM (n = 11 cells per compound). Effects of baclofen versus peptide are analyzed using Paired t-test (two-tailed. ***$p < 0.001$ and ****$p < 0.0001$) and mean ± SEM are shown alongside.

Fig. 5. Inhibition of wild-type and mutant $GABA_BR$-coupled Cav2.2 channels expressed in HEK293T cells by analgesic α-conotoxins Vc1.1, Rg1A, and PeIA. **(A) (i)** Vc1.1 (1 μM) inhibition of baclofen-sensitive I_{Ba} amplitude mediated by human Cav2.2 channel co-transfected with wild-type (WT) $GABA_BR$. Bar graph of the effect of 1 μM Vc1.1 on the baclofen-sensitive I_{Ba} in HEK293T cells over-expressing S130A, S131A, S153A, S154A, S130A+S153A, R162A, T198A, E200A, E253A, F227A, and D380A mutants of $GABA_BR$ B1 subunit and R89A, D165A, K168A or R207A mutants of $GABA_BR$ B2 subunit. Dashed line indicates inhibition of baclofen-sensitive I_{Ba} by Vc1.1 with WT $GABA_BR$. **(ii)** Superimposed whole-cell I_{Ba} mediated by $GABA_BR$-coupled Cav 2.2 channels in absence (control, black) and presence of 1 μM Vc1.1 (blue), and 100 μM baclofen (grey). Overexpression of the double mutant (S130A + S153A) abolished the inhibition of $GABA_BR$-coupled Cav2.2 channels by both baclofen and Vc1.1. **(B) (i)** Rg1A (1 μM) inhibition of baclofen-sensitive I_{Ba} amplitude of hCav2.2 channel co-transfected with WT $GABA_BR$. Bar graph of the effect of 1 μM RgIA on the baclofen-sensitive I_{Ba} in HEK293T

Molecular Pharmacology Fast Forward. Published on August 9, 2022 as DOI: 10.1124/molpharm.122.000543
This article has not been copyedited and formatted. The final version may differ from this version.

cells over-expressing S130A, S131A, S153A, S154A, S130A+S153A, R162A, E200A, E253A, F227A, and D380A of the B1 subunit and R89A, D165A, K168A or R207A mutants of the B2 subunit. Dashed line indicates inhibition of baclofen-sensitive current by Rg1A with WT $GABA_BR$. **(ii)** Superimposed whole-cell I_{Ba} mediated by $GABA_BR$-coupled Cav 2.2 channels in absence (control, black) and presence of 1 μM Rg1A (green) and 100 μM baclofen. Similarly, over-expression of the double mutant (S130A + S153A) abolished Rg1A and baclofen inhibition of $GABA_BR$-coupled Cav2.2 channels. **(C) (i)** PeIA (1 μM) inhibits baclofen-sensitive I_{Ba} current amplitude of Cav2.2 channel transfected with WT-$GABA_BR$ in HEK293 cells to 57.5 ± 3.2% (n = 11). Bar graph of the effect of 1 μM PeIA on the baclofen-sensitive I_{Ba} in HEK293T cells over-expressing S130A, S131A, S153A, S154A, S130A+S153A, R162A, E200A, E253A, F227A, and D380A of the B1 subunit and R89A, D165A, K168A, or R207A mutants of the B2 subunit. Dashed line indicates inhibition of baclofen-sensitive current by Pe1A with WT $GABA_BR$. **(ii)** Superimposed whole-cell I_{Ba} mediated by $GABA_BR$-coupled Cav 2.2 channels in the absence (control, black) and presence of 1 μM PeIA (purple) and 100 μM baclofen (grey). Overexpression of the double mutant abolished the inhibition of I_{Ba} by PeIA. Data represent mean ± S.E.M. One-way ANOVA followed by Dunnett's post hoc test. Statistical significance, **** $p < 0.0001$ vs WT-$GABA_BR$, *** $P < 0.0005$, ** $P < 0.005$ and * $p < 0.05$.

Fig. 6. Representative fluorescent micrographs of double-immunostaining of $GABA_BR$ subunits for WT and receptors mutated at residues predicted to form close contact with analgesic α-conotoxins. Left panel: Visualisation of the $GABA_BR2$-eGFP subunit from WT and 4 individual mutants of $GABA_BR$ when overexpressed recombinantly in HEK293T cells. Middle panels: Anti-$GABA_BB1$ (cyan) and anti-$GABA_BB2$ (red) staining of expressed receptor, illustrating expression of both subunits that are co-localised (merged) with each other when visualised in confocal microscopy. Right panel: DIC light microscope images of corresponding HEK293T cells. Scale bars 100 μm.

Fig. 7. Simulation and docking-predicted binding location and functional analysis for RgIA and its analogue RgIA4 at $GABA_BR$. **(A)** Docking-predicted poses of the analogue RgIA (top) and RgIA4 (bottom) bound at the initial 4MQF structure, with the α-conotoxins shown as large spheres at the inter-subunit region of the VFT (blue = B1, red = B2). Residues previously predicted to form close contacts with Vc1.1, RgIA, and PeIA at the B1 subunit

Molecular Pharmacology Fast Forward. Published on August 9, 2022 as DOI: 10.1124/molpharm.122.000543
This article has not been copyedited and formatted. The final version may differ from this version.

and whose Ala mutants result in significantly reduced inhibition of baclofen-sensitive current are shown as blue spheres. RgIA4 is known to be inactive at $GABA_BR$, and docking predicts that it preferentially binds towards the B2 side of the interface, while only partly forming contacts with the main B1 agonist/antagonist site, in contrast to RgIA which binds primarily to the B1 site. **(B) (i)** Rg1A4 (1 μM) had no significant effect on baclofen-sensitive I_{Ba} amplitude of hCav2.2 channel co-transfected with WT $GABA_BR$. I_{Ba} amplitude was reduced by < 20% (n = 5) by 1 μM RgIA4 compared to Rg1A (1 μM). **(ii)** Superimposed whole-cell HVA I_{Ba} currents mediated by $GABA_BR$-coupled Cav 2.2 in the absence (control, black) and presence of 1 μM Rg1A4 (light green) and 100 μM baclofen (grey).

Fig. 8. α-Conotoxin-induced $GABA_BR$ conformation shifts predicted by MD. (A) Time series plots of B1 inter-lobe distances for $GABA_BR$ bound with Vc1.1 (blue line), RgIA (green), and PeIA (purple) measured by I286 and E343 separation. The inter-lobe separation for apo-$GABA_BR$ is shown by a horizontal black line, while the separation for the baclofen-bound VFT crystal structure (4MS4) is shown with a dashed black line. **(B)** Time series plots of B1/B2 inter-subunit distances for $GABA_BR$ bound with Vc1.1 (blue line), RgIA (green), and PeIA (purple) measured by B1-R239 and B2-E230 separation. The B1/B2 separation for apo-$GABA_BR$ is shown by a horizontal black line, while the separation for the baclofen-bound VFT crystal structure (4MS4) is shown with a dashed black line. Graphical insets on the right-hand side show representative structures of the VFT bound with baclofen (grey) or the α-conotoxins.

Molecular Pharmacology Fast Forward. Published on August 9, 2022 as DOI: 10.1124/molpharm.122.000543
This article has not been copyedited and formatted. The final version may differ from this version.

Table 1. Inhibition of baclofen-sensitive Ba^{2+} current (% $I_{peptide}/I_{baclofen}$) mediated by wild-type (WT) and mutant $GABA_BR$-coupled Cav2.2 channels expressed in HEK293T cells by α-conotoxins Vc1.1, Rg1A, and PeIA.

$GABA_BR$ mutants	**Vc1.1**		**Rg1A**		**PeIA**	
WT-$GABA_BR$	59 ± 4 (11)	+++	54 ± 3 (11)	+++	58 ± 3 (11)	+++
B1 subunit						
S130A	33 ± 4 (9)	++	31 ± 7 (5)	++	38 ± 3 (5)	++
S131A	39 ± 5 (6)	++	40 ± 5 (5)	++	16 ± 4 (6)	++
S153A	12 ± 2 (9)	+	13 ± 3 (5)	+	19 ± 1 (5)	+
S154A	17 ± 2 (5)	+	16 ± 5 (5)	+	28 ± 5 (5)	++
S130A+S153A	11 ± 2 (9)	–	11 ± 3 (5)	–	7 ± 2 (5)	–
R162A	19 ± 4 (5)	+	9 ± 1 (5)	+	16 ± 2 (5)	+
T198A	30 ± 2 (5)	++	31 ± 1 (5)	++	30 ± 2 (5)	++
E200A	22 ± 4 (5)	++	17 ± 5 (5)	+	16 ± 2 (5)	+
E253A	23 ± 5 (5)	++	26 ± 4 (5)	++	43 ± 7 (5)	++
F227A	23 ± 3 (5)	++	16 ± 3 (5)	+	19 ± 3 (5)	+
D380A	52 ± 2 (5)	+++	47 ± 4 (5)	+++	46 ± 4 (5)	+++
B2 subunit						
R89A	46 ± 3 (5)	+++	51 ± 4 (5)	+++	48 ± 4 (5)	+++
D165A	27 ± 4 (5)	++	31 ± 2 (5)	++	30 ± 1 (5)	++
K168A	15 ± 5 (5)	+	21 ± 3 (6)	++	9 ± 3 (5)	+
R207A	20 ± 5 (5)	++	16 ± 3 (5)	+	14 ± 3 (5)	+

+++ Maximum inhibition (> 45%) of WT and mutant $GABA_BR$-coupled Cav2.2 channels by baclofen (50 μM) and α-conotoxins (1 μM)

++ Reduced inhibition (20 - 45%) of baclofen-sensitive current

\+ Significantly reduced inhibition (< 20%) of baclofen-sensitive current

– No inhibition of baclofen-sensitive current

Whole-cell I_{Ba} mediated by the double mutant S130A+S153A was inhibited by the selective Cav2.2 antagonist, ω-conotoxin CVIE (100 nM).

Molecular Pharmacology Fast Forward. Published on August 9, 2022 as DOI: 10.1124/molpharm.122.000543
This article has not been copyedited and formatted. The final version may differ from this version.

Figure 1

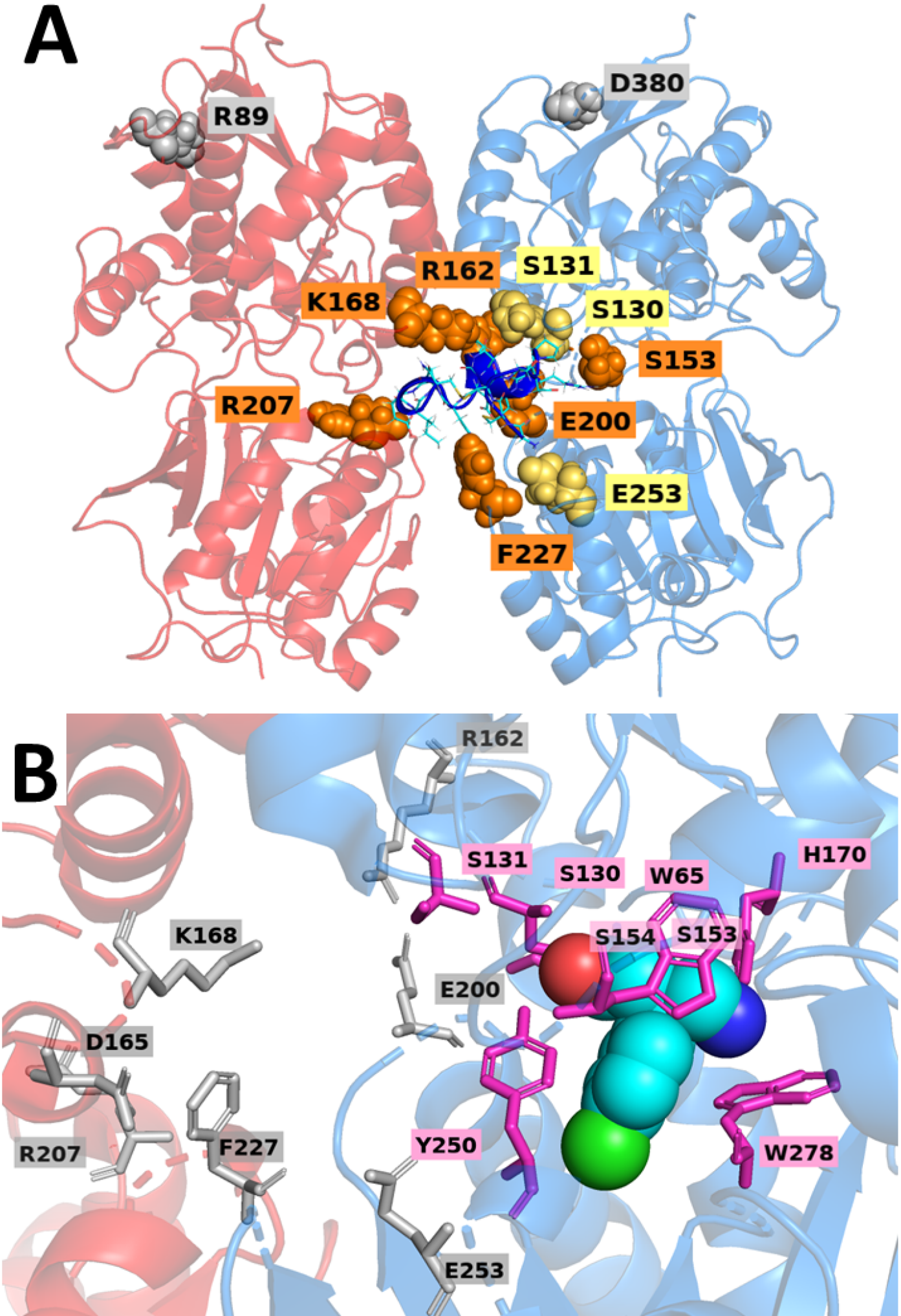

Molecular Pharmacology Fast Forward. Published on August 9, 2022 as DOI: 10.1124/molpharm.122.000543
This article has not been copyedited and formatted. The final version may differ from this version.

Figure 2

Vc1.1-GABA$_B$R

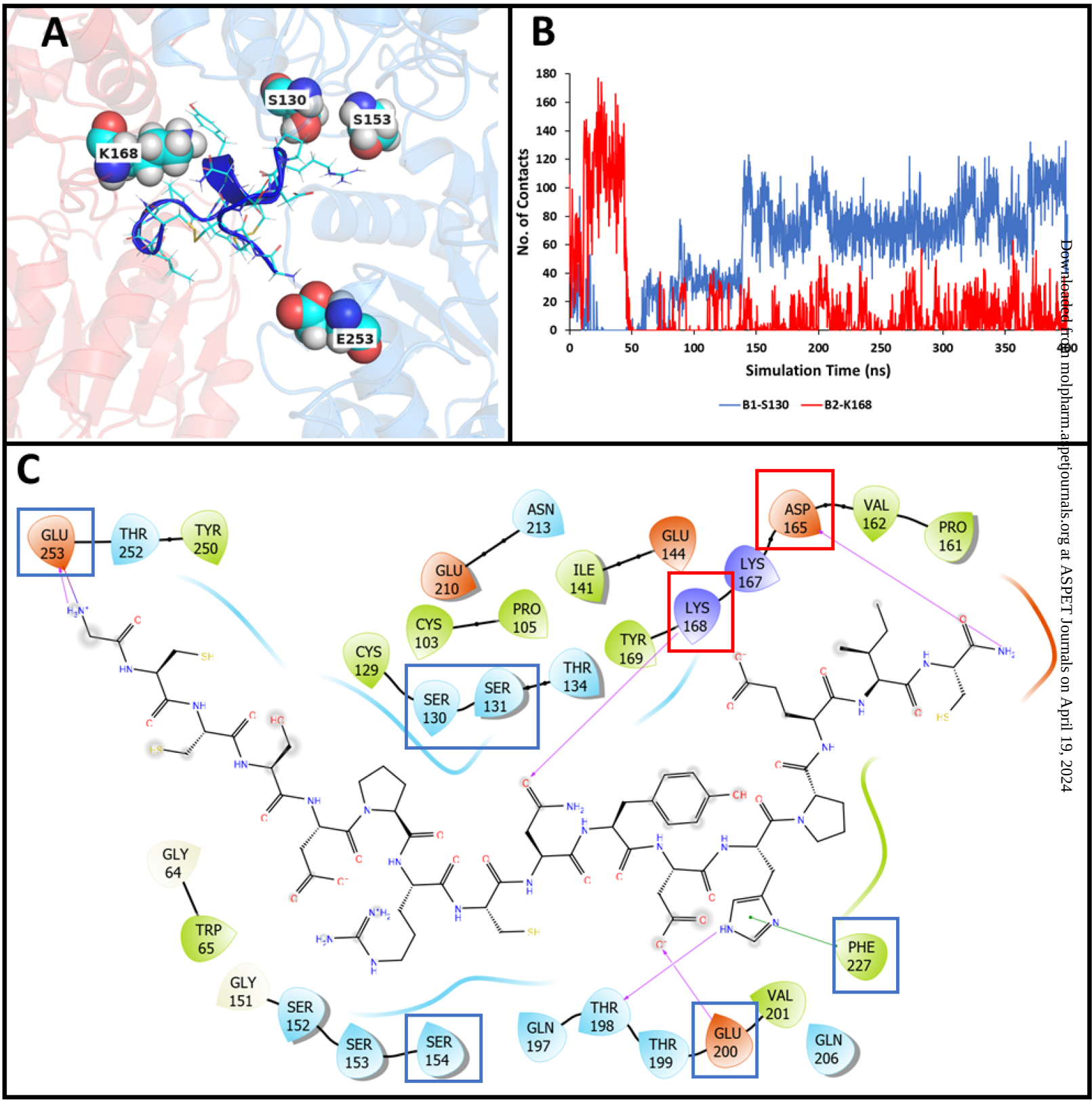

Molecular Pharmacology Fast Forward. Published on August 9, 2022 as DOI: 10.1124/molpharm.122.000543
This article has not been copyedited and formatted. The final version may differ from this version.

Figure 3

RgIA-GABA$_B$R

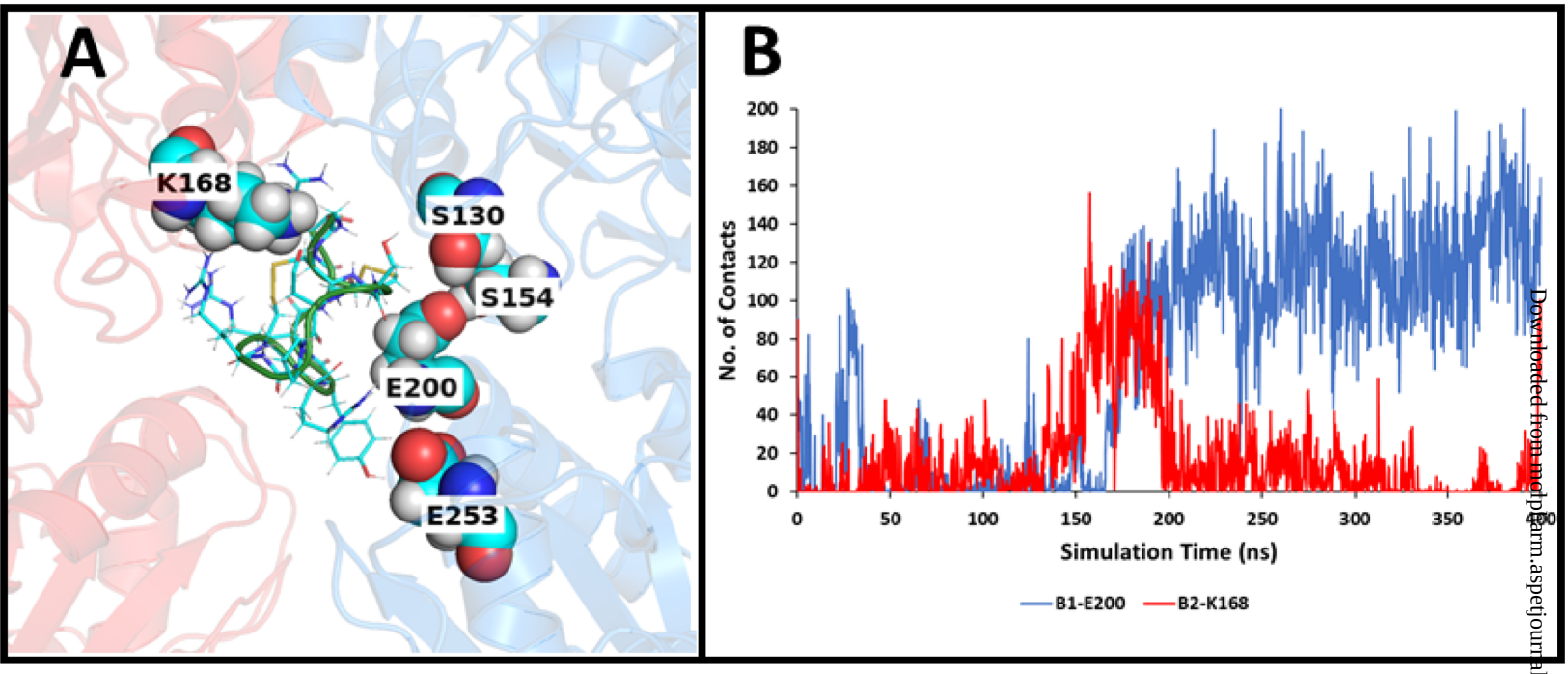

PeIA-GABA$_B$R

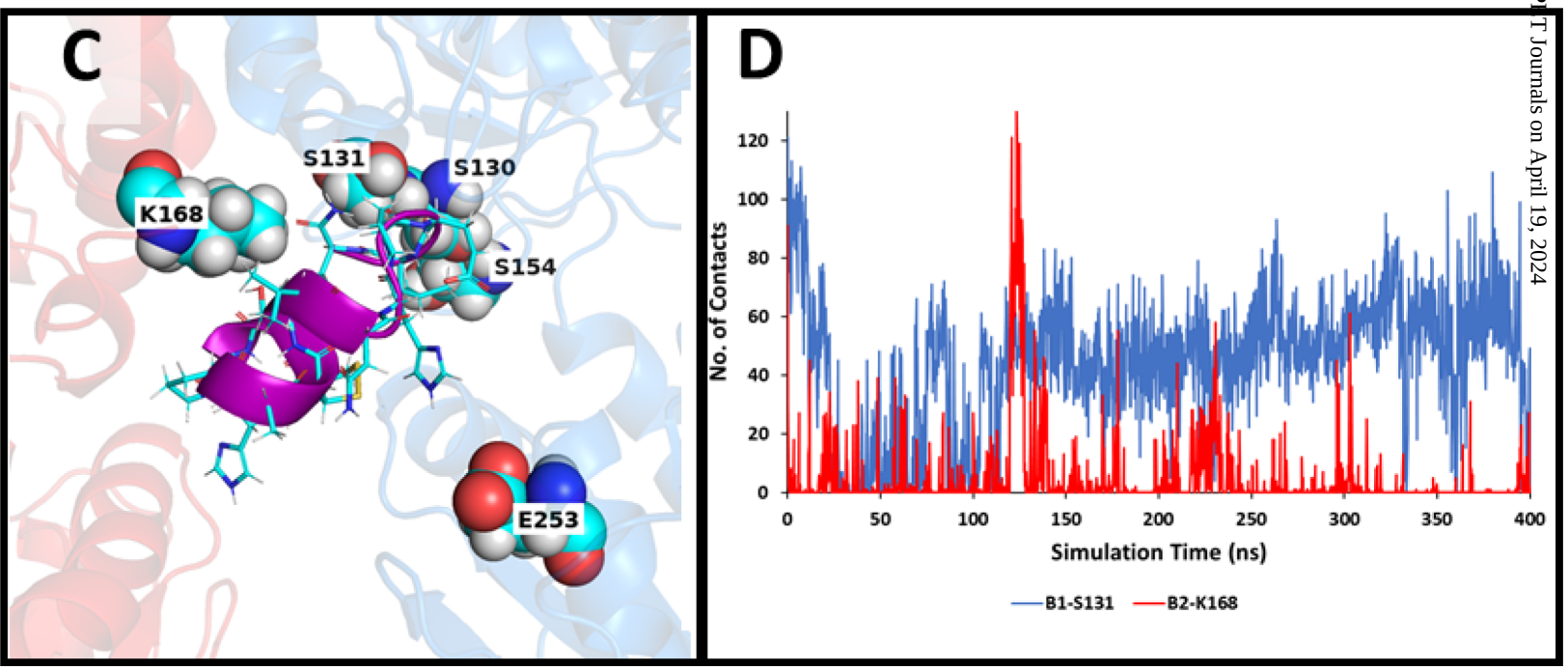

Molecular Pharmacology Fast Forward. Published on August 9, 2022 as DOI: 10.1124/molpharm.122.000543
This article has not been copyedited and formatted. The final version may differ from this version.

Figure 4

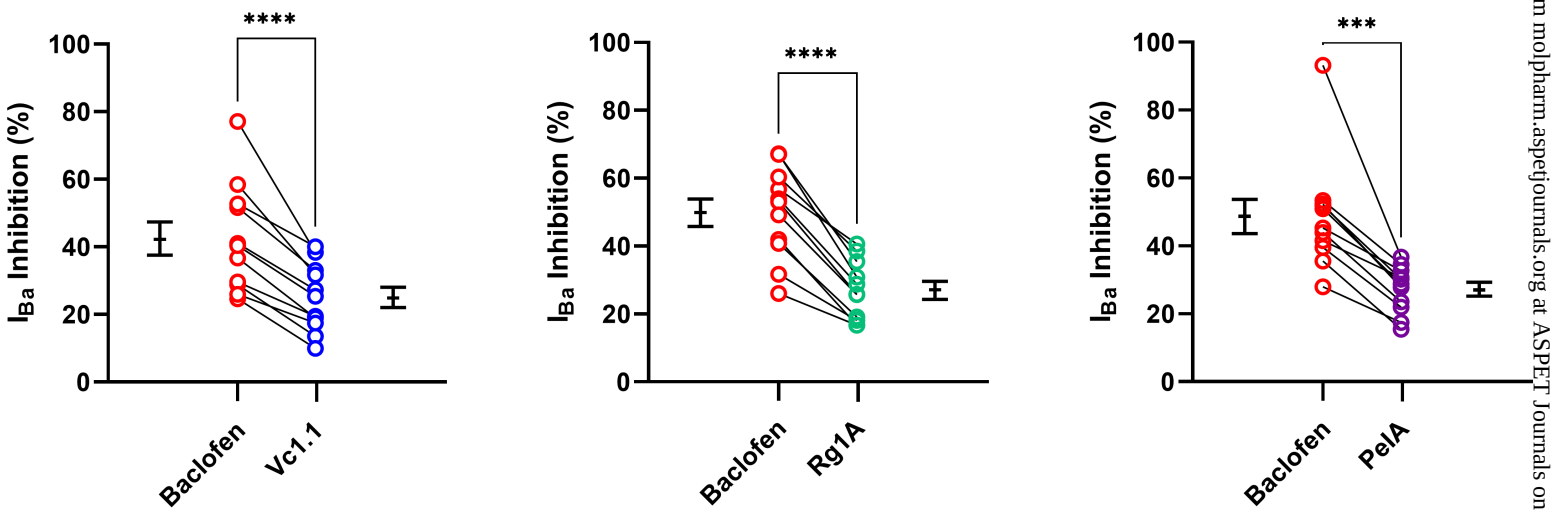

Molecular Pharmacology Fast Forward. Published on August 9, 2022 as DOI: 10.1124/molpharm.122.000543
This article has not been copyedited and formatted. The final version may differ from this version.

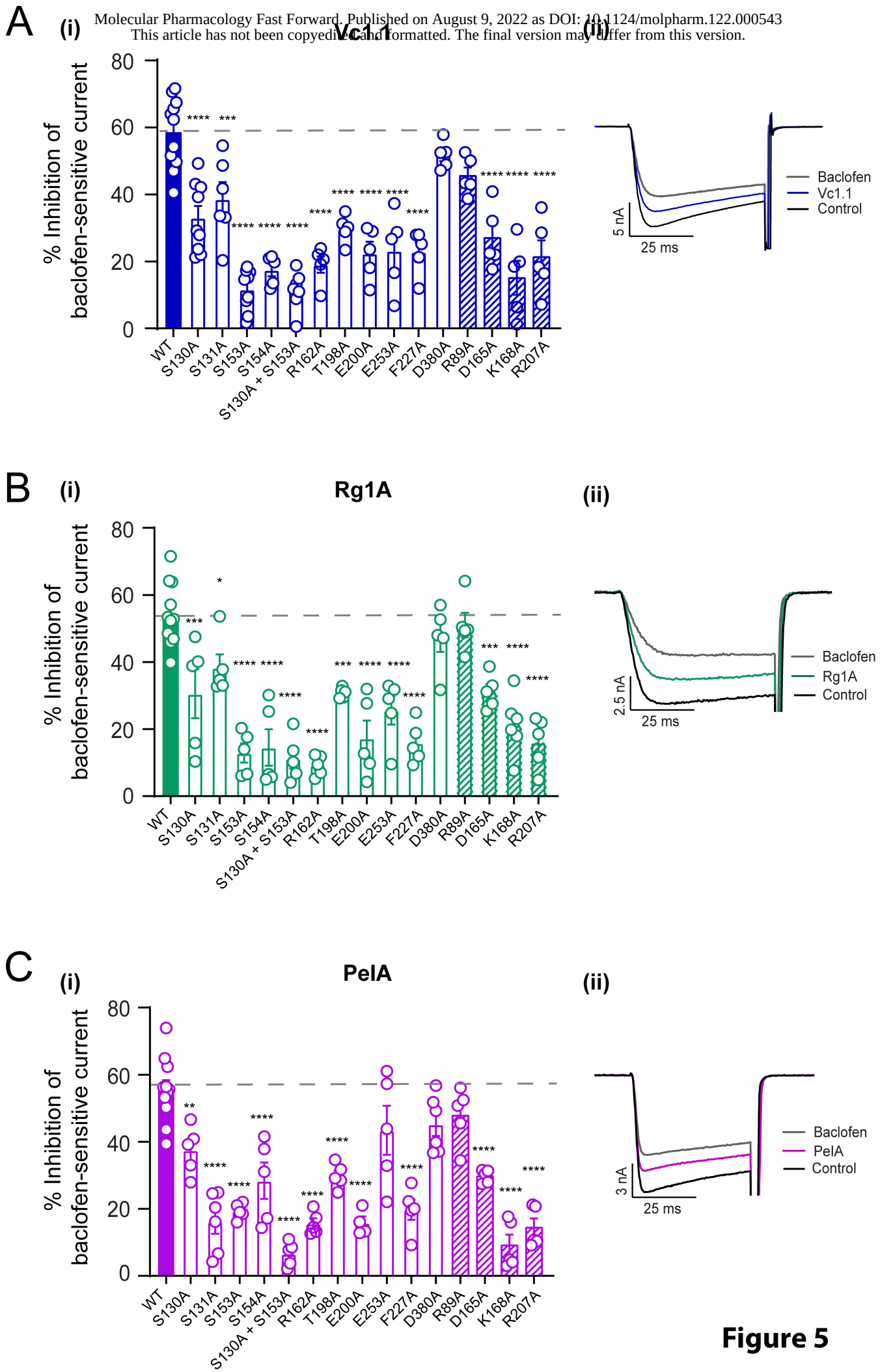

Figure 5

Molecular Pharmacology Fast Forward. Published on August 9, 2022 as DOI: 10.1124/molpharm.122.000543
This article has not been copyedited and formatted. The final version may differ from this version.

Figure 6

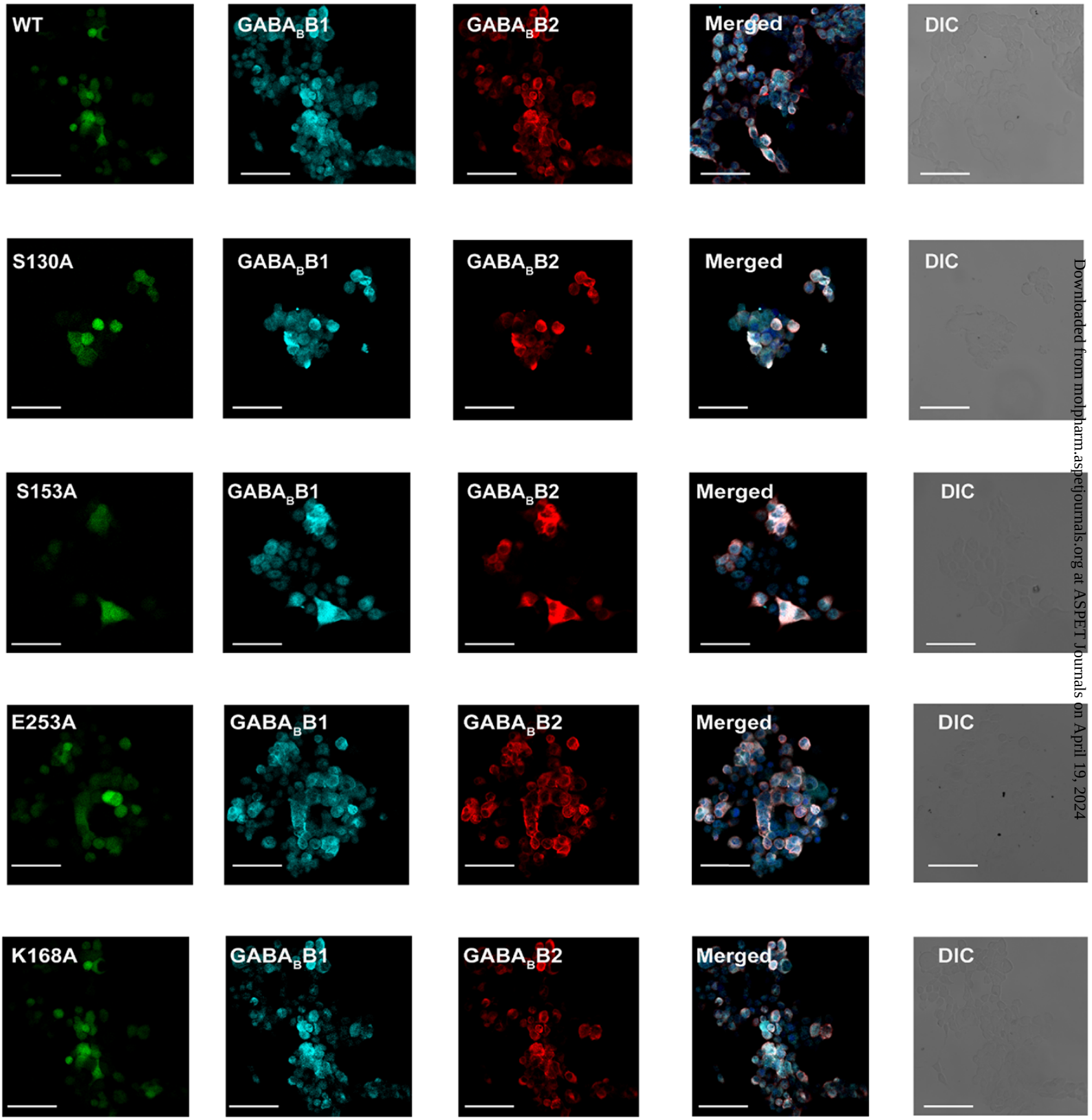

Molecular Pharmacology Fast Forward. Published on August 9, 2022 as DOI: 10.1124/molpharm.122.000543
This article has not been copyedited and formatted. The final version may differ from this version.

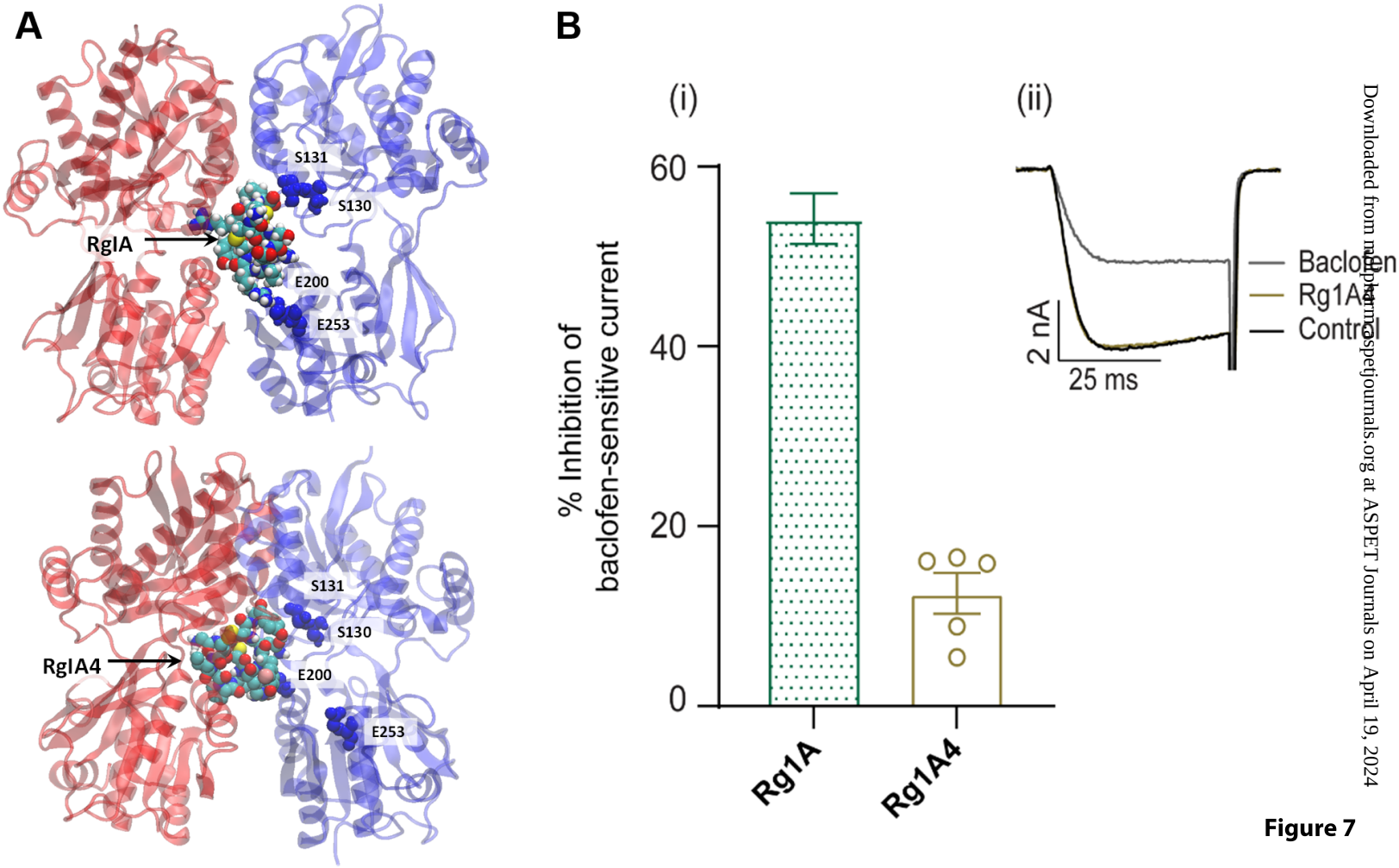

Figure 7

Molecular Pharmacology Fast Forward. Published on August 9, 2022 as DOI: 10.1124/molpharm.122.000543
This article has not been copyedited and formatted. The final version may differ from this version.

Figure 8